Supporting Information for

Stretchable $Ti_3C_2T_x$ MXene Microsupercapacitors with High Areal Capacitances and Quasi-Solid-State Multivalent Neutral Electrolyte

Shuo Li [a1], Ting-Hsiang Chang [a1], Yang Li [a], Meng Ding [a], Po-Yen Chen [b,*]

[a] Department of Chemical and Biomolecular Engineering, National University of Singapore, 117585 Singapore

[b] Department of Chemical and Biomolecular Engineering, University of Maryland, College Park, MD, 20742

Email: checp@umd.edu

Experimental Section

Materials. Lithium fluoride (LiF, ≥99.0%), hydrochloric acid (HCl, 37%), sulfuric acid (H_2SO_4, 98%), poly(vinyl alcohol) (PVA, average M_w ~130,000), zinc sulfate heptahydrate ($ZnSO_4 \cdot 7H_2O$), dichloromethane (DCM, 99.9%), gelatin from water fish skin, tetrahydrofuran (THF, ≥99.0%), xylene (≥98.5%), toluene (99.8%), chloroform (CF, 99.9%), *N,N*-dimethylformamide (DMF, ≥99.8%), and glutaraldehyde solution (25 vol.% in H_2O) were purchased from Sigma-Aldrich and used as received without further purification. Ti_3AlC_2 MAX phase powders (500 mesh) were purchased from Laizhou Kai Kai Ceramic Materials Co Ltd. Clear polystyrene (PS) heat shrink films were purchased from Grafix. Silicone elastomer, Ecoflex™-0050, was purchased from Smooth-On. Deionized (DI) water (18.2 MΩ) was obtained from a Milli-Q water purification system (Millipore Corp., Bedford, MA, USA) and used as the water source throughout the work.

Preparation of $Ti_3C_2T_x$ MXene nanosheets. $Ti_3C_2T_x$ MXene nanosheets were prepared by etching Al of Ti_3AlC_2 MAX according to the literature with some modifications.[1] In brief, $Ti_3C_2T_x$ MAX powders (1.0 g) were slowly added into a mixture composed of LiF (3.0 g) and 9.0 M HCl (40 mL) within 5 minutes, then stirred at 35 °C with 400 rpm for 24 hours. Afterwards, the solid residue was washed with DI water through repeated centrifuges at 8,000 rpm for 5 minutes each until the pH value increased to 6.0. Subsequently, the washed residuals were added into 60 mL of DI water, ultrasonicated for 30 minutes under N_2 protection in an ice bath, and further centrifuged at 3,000 rpm for 20 minutes. The supernatant was collected as the final dispersion of MXene nanosheets with the concentration of ca. 10 mg mL^{-1}.

Fabrication of MXene SMSCs. A clear shrink film was first cut into multiple 3 cm × 4 cm rectangles, and a Kapton mask with interdigitated electrode pattern was attached onto the cut shrink film. Afterwards, the masked shrink film was treated with oxygen plasma in a Harrick plasma cleaner for 2 minutes, and the MXene nanosheet dispersion was deposited on the shrink film at an areal mass loading of 0.36 mg cm^{-2} followed by overnight drying at room temperature. After removing the Kapton mask, the planar MXene/PS device was heated in an oven above the T_g of PS (at 140 °C) for 5 minutes to induce the thermal shrinkage of PS substrate. The shrunk MXene/PS device was then deposited with uncured

Ecoflex *via* spin coating at 500 rpm for 30 seconds, followed by curing at room temperature for 4 hours. The shrunk MXene/PS device with Ecoflex backing was then immersed in a DCM bath to dissolve the PS substrate. After the PS substrate was completely dissolved, the MXene/Ecoflex device was sequentially rinsed with DCM, acetone, and ethanol, followed by overnight drying at room temperature.

A quasi-solid-state acidic electrolyte was prepared by adding PVA into H_2SO_4 solution according to the literature.[2] In detail, 1.0 g of PVA was dissolved into 10 mL of DI water, and the mixture was heated up to 90 °C under vigorous stirring until the mixture became clear. 3.0 g of H_2SO_4 (98%) was added drop-wise, followed by continuous stirring for 1 hour. The gel electrolyte of PVA/H_2SO_4 was then cast onto e-MXene device for the fabrication of e-MXene H^+-SMSCs.

A quasi-solid-state neutral electrolyte was composed of 1.0 M $ZnSO_4$, 15.0 w/v% of gelatin, and 2.0 v/v% of glutaraldehyde solution, which was applied to fabricate e-MXene Zn^{2+}-SMSCs.[3] In detail, 1.5 g of gelatin powders were dissolved into 10 mL of 1.0 M $ZnSO_4$ solution under vigorous stirring at 60 °C until the mixture becomes clear. The gelatin/$ZnSO_4$ solution was subsequently mixed with 20 μL of glutaraldehyde solution and quickly poured on the top of e-MXene device. Both e-MXene H^+-SMSC and e-MXene Zn^{2+}-SMSC were placed in a vacuum desiccator to remove air bubbles, and the gel electrolytes were able to be infiltrated into higher dimension MXene micro-textures.

Electrochemical characterizations of e-MXene H^+-SMSCs and e-MXene Zn^{2+}-SMSCs. The fabricated e-MXene H^+-SMSCs and e-MXene Zn^{2+}-SMSCs were next characterized by an electrochemical workstation (Autolab PGSTAT302N) at room temperature. Cyclic voltammetry (CV) and galvanostatic charge−discharge (GCD) measurements were conducted to evaluate their electrochemical performance. The areal-specific capacitance (C_A) of these MXene SMSCs were evaluated from their CV curves by using **Equation S1**,

$$C_A = \frac{1}{\Delta V s} \int j dV \quad \text{(S1)}$$

, where j is the discharge current density (A cm^{-2}), $\int j\, dV$ is the integrated area of CV curves, ΔV is the potential window (V), and s is the scan rate (V s^{-1}). The C_A of these MXene SMSCs was further validated from their GCD curves by using **Equation S2**,

$$C_A = \frac{I \times \Delta t}{A \times \Delta V} \quad \text{(S2)}$$

, where I is the discharging current (A), Δt is the discharging time (s), and A is the dimensions of SMSC (cm^2). The electrochemical impedance spectroscopy (EIS) measurement was conducted at an open circuit potential (OCP), with an amplitude of 5 mV and varying frequencies from 0.1 Hz to 100 kHz. For the Ragone plot, the areal energy density and areal power density of e-MXene SMSC were calculated by using **Equation S3** and **S4**,

$$E_D = \frac{C_A \times \Delta V^2}{2 \times 3.6} \quad \text{(S3)}$$

$$P_D = \frac{E_D \times 3600}{\Delta t} \quad \text{(S4)}$$

, where E_D is the areal energy density of e-MXene SMSCs (mWh cm^{-2}), P_D is the areal power density of e-MXene SMSCs (mW cm^{-2}), ΔV is the voltage window (V), and Δt discharge time (second).

Material characterizations. The surface morphologies of MXene SMSCs were obtained using a scanning electron microscope (SEM, FEI Quanta 600) and a field emission SEM (JEOL-JSM-6610LV) operating at 15.0 kV. The morphology of MXene nanosheets was measured by applying a high-resolution transmission electron microscopy (HRTEM, JEOL 2010F). The X-ray diffraction (XRD) patterns of planar MXene nanolayer, crumple-textured MXene nanolayer, and e-MXene device were recorded by an X-ray diffractometer (XRD, Bruker, D8 Advance X-ray Powder Diffractometer, Cu Kα (λ = 0.154 nm) radiation) with a scan rate of 2° min^{-1}. X-ray photoelectron spectra (XPS) of MXene nanocoatings were recorded on an X-ray photoelectron spectrometer (Kratos AXIS UltraDLD) *via* a microfocused Al X-ray beam (100 μm, 25 W), with a photoelectron take off angle of 90°. Particle size distributions were measured using dynamic light scattering (DLS, Malvern Nano ZetaSizer Analyzer). The atomic force microscope (AFM) images of MXene nanosheets were captured on a Bruker Dimension ICON microscope. Thicknesses of planar MXene nanolayers were measured using a surface profiler (Alpha-Step IQ). *I–V* profiles of planar MXene nanolayer, crumple-textured MXene nanolayer, and e-MXene device were measured by using an electrochemical workstation (Autolab PGSTAT302N) at room temperature. The tensile tests were measured by using a universal testing system (Instron

5567, Instron, Canton, MA), and the uniaxial strains applied to e-MXene H^+-SMSC and e-MXene Zn^{2+}-SMSC were defined as **Equation S5**,

$$Uniaxial\ Strain = \frac{L_s - L_0}{L_0} \quad \text{(S5)}$$

, where L_0 is the original length of SMSCs, and the L_s is the length of SMSCs at various stretching states.

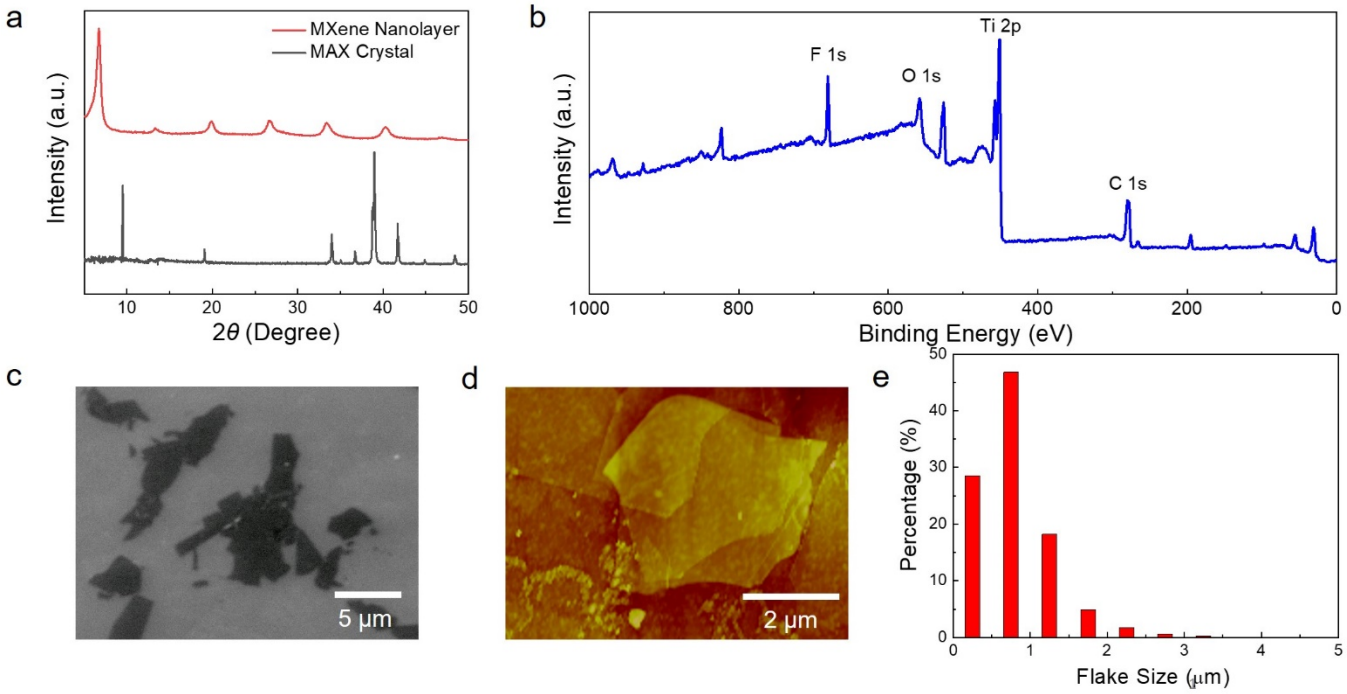

Fig S1. Characterization of $Ti_3C_2T_x$ MXene nanosheets. (a) XRD patterns of Ti_3AlC_2 MAX crystals and $Ti_3C_2T_x$ MXene nanolayers. (b) XPS survey scan of $Ti_3C_2T_x$ MXene nanolayers. (c) High-resolution SEM image of as-exfoliated $Ti_3C_2T_x$ MXene nanosheets. (d) AFM image of $Ti_3C_2T_x$ MXene nanosheets. (e) Flake size distribution of $Ti_3C_2T_x$ MXene dispersion.

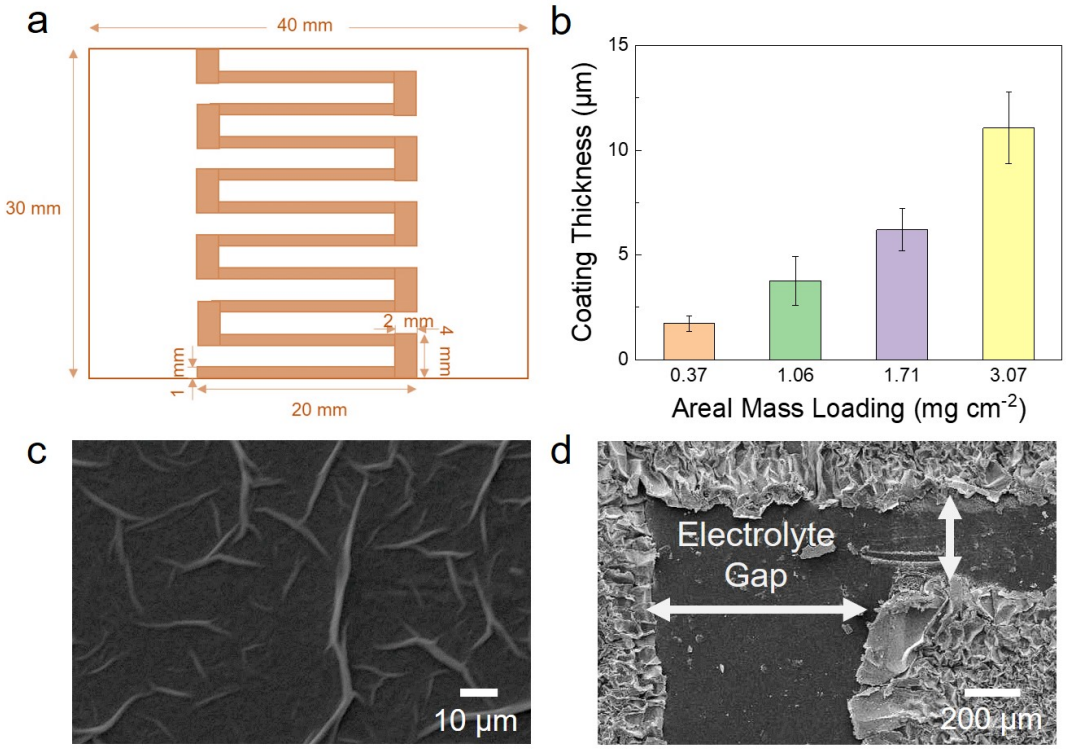

Fig S2. (a) Dimensions of a polyester mask used to fabricate planar MXene/PS devices. MXene dispersion was deposited onto the unmasked region. (b) Thickness of MXene coating as a function of areal mass loading of MXene nanosheets. (c) SEM image of the planar MXene electrode deposited onto PS substrate. (d) SEM image of a shrunk MXene/PS device with an average electrode finger width of 1.0 mm and an average electrolyte gap of 0.35 mm.

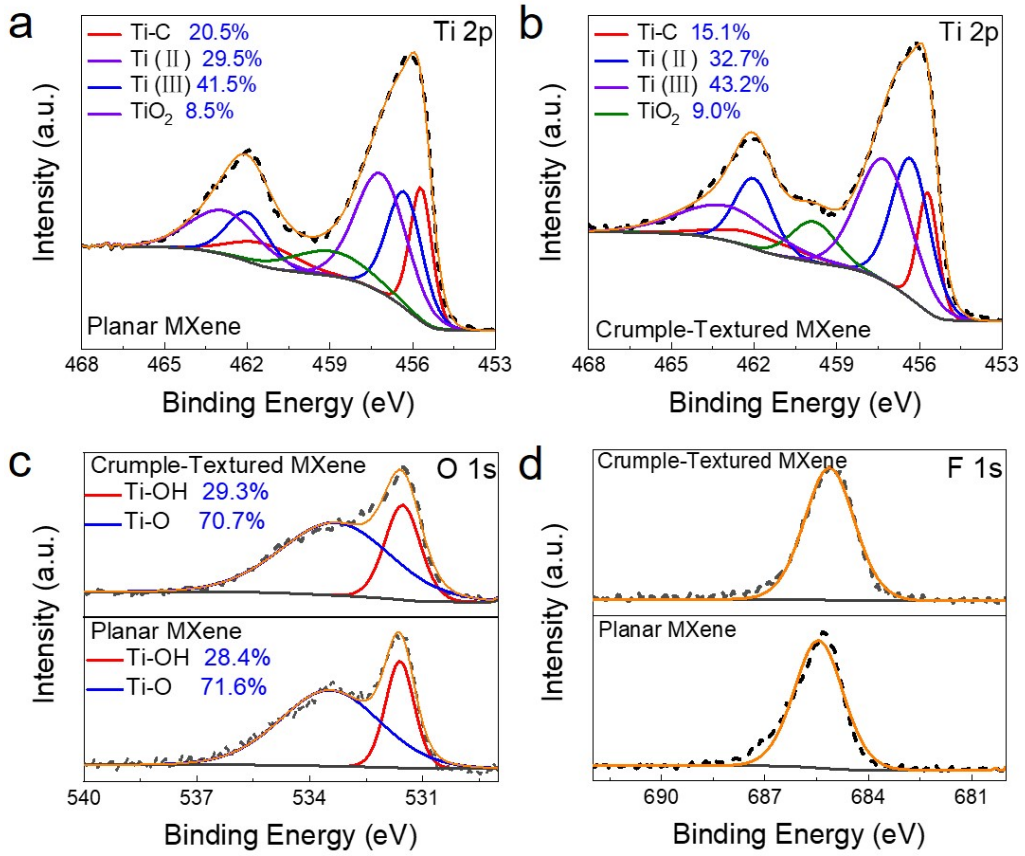

Fig S3. Ti 2p XPS spectra of (a) planar and (b) crumple-textured MXene coatings. The component's contributions are listed in the legends. (c) O 1s XPS spectra of planar and crumple-textured MXene coatings. The component's contributions are listed in the legends. (d) F 1s XPS spectra for planar and crumple-textured MXene coatings.

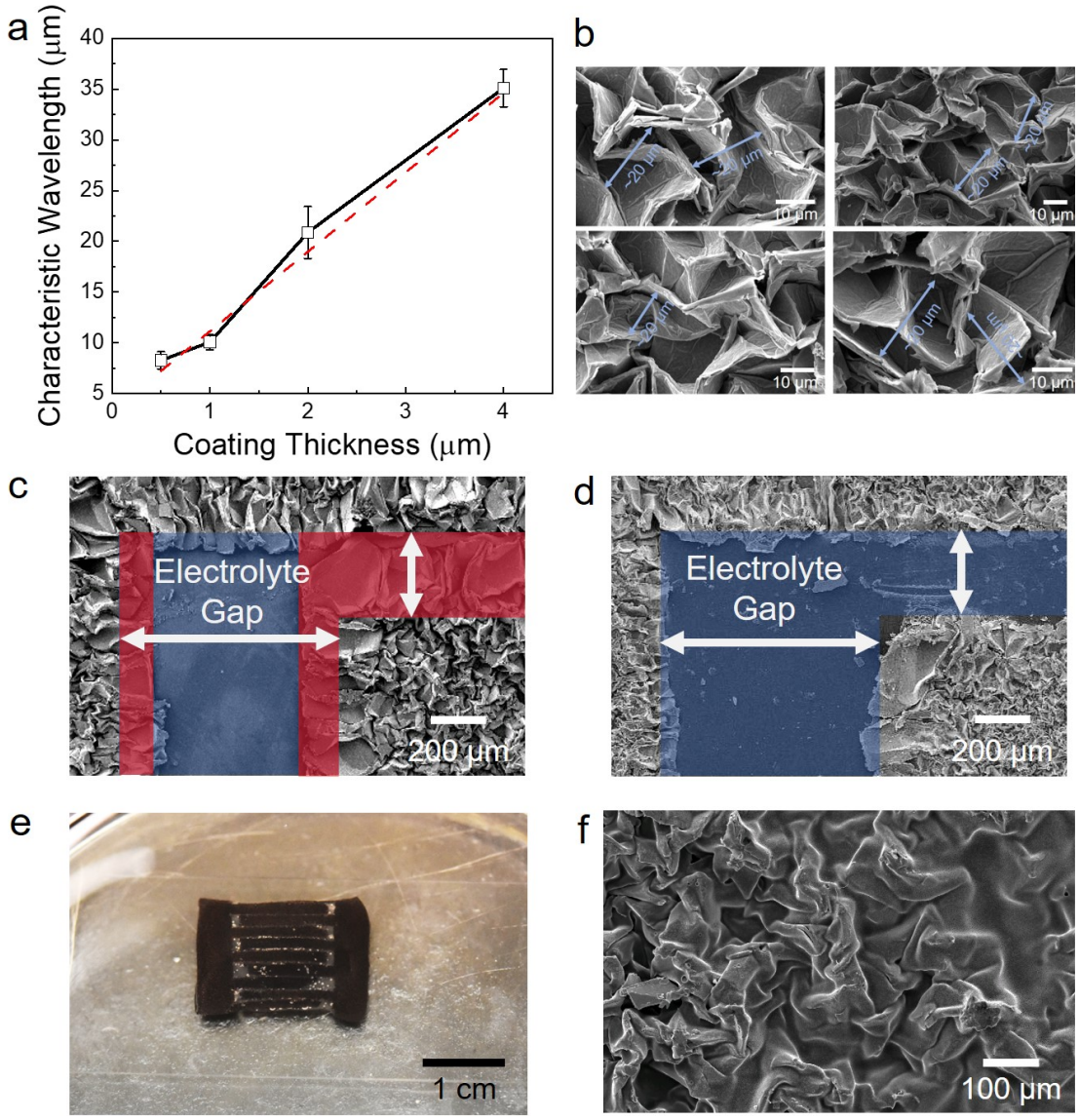

Fig S4. (a) Average characteristic wavelength of crumple-textured MXene nanolayer was controlled by the thickness of planar MXene nanolayer. (b) High-resolution SEM images of crumple-textured MXene coating with mass loading of 0.36 mg mL^{-1}, and the characteristic wavelength of MXene crumples was extracted to be ~20 μm, which was defined as the whole crumple size measured in multiple SEM images. (c) SEM image of a shrunk MXene/PS device with a higher areal mass loading of 0.54 mg cm^{-2} (electrode thickness of ~2.2 μm). Open electrolyte gap was highlighted in blue, and unfavorable MXene coverage of electrolyte gap was highlighted in red. (d) SEM image of a shrunk MXene/PS device with an optimal areal mass loading of 0.36 mg cm^{-2} (electrode thickness

of ~1.5 μm). Open electrolyte gap was highlighted in blue. (e) Digital photograph of a swollen e-MXene device in a DCM bath. (f) SEM image of an e-MXene device fabricated by a lower speed of spin coating at 100 rpm. The crumple-textured MXene nanolayer was partially embedded within Ecoflex matrix, and higher electrical resistances were shown in the resulting e-MXene electrodes.

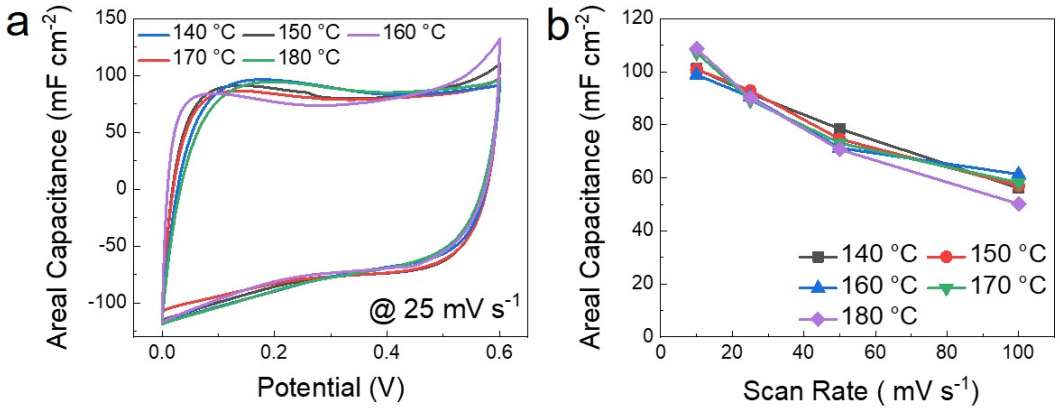

Fig S5. (a) CV curves of crumple-textured MXene MSCs obtained at various heating temperatures ranging from 140 °C to 180 °C at 25 mV s^{-1}. (b) C_A of crumple-textured MXene MSCs fabricated at different heating temperatures at the scan rates varying from 10 to 100 mV s^{-1}.

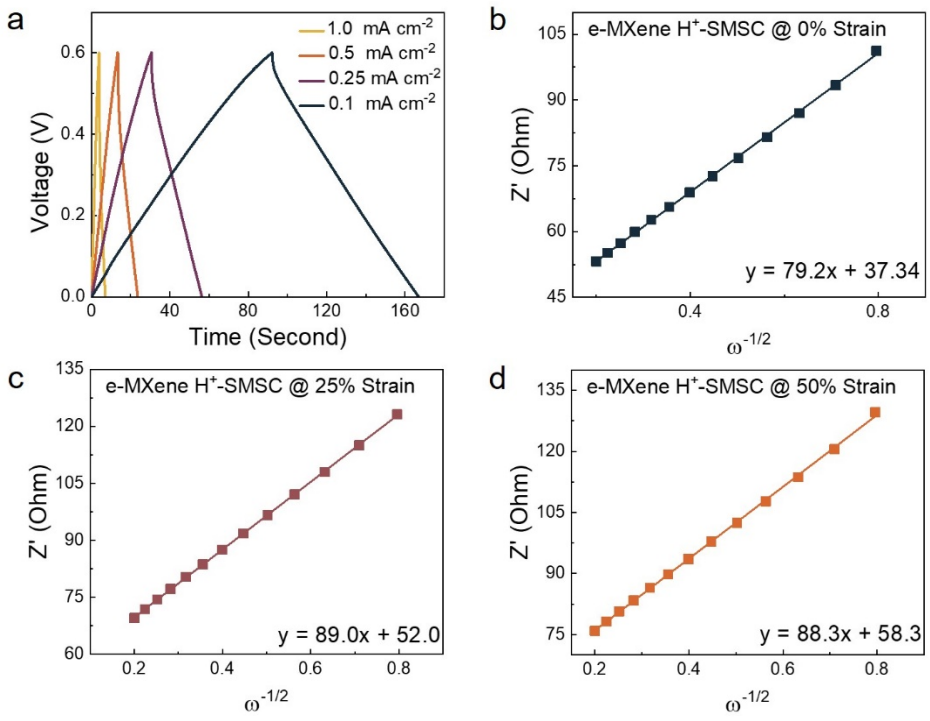

Fig S6. (a) GCD profiles of a planar MXene MSC at different charge-discharge current densities (0.10, 0.25, 0.50, 1.00 mA cm^{-2}). Linear relations were observed between Z' and $\omega^{-1/2}$ of an e-MXene H^+-SMSC under (b) 0%, (c) 25%, and (d) 50% strains.

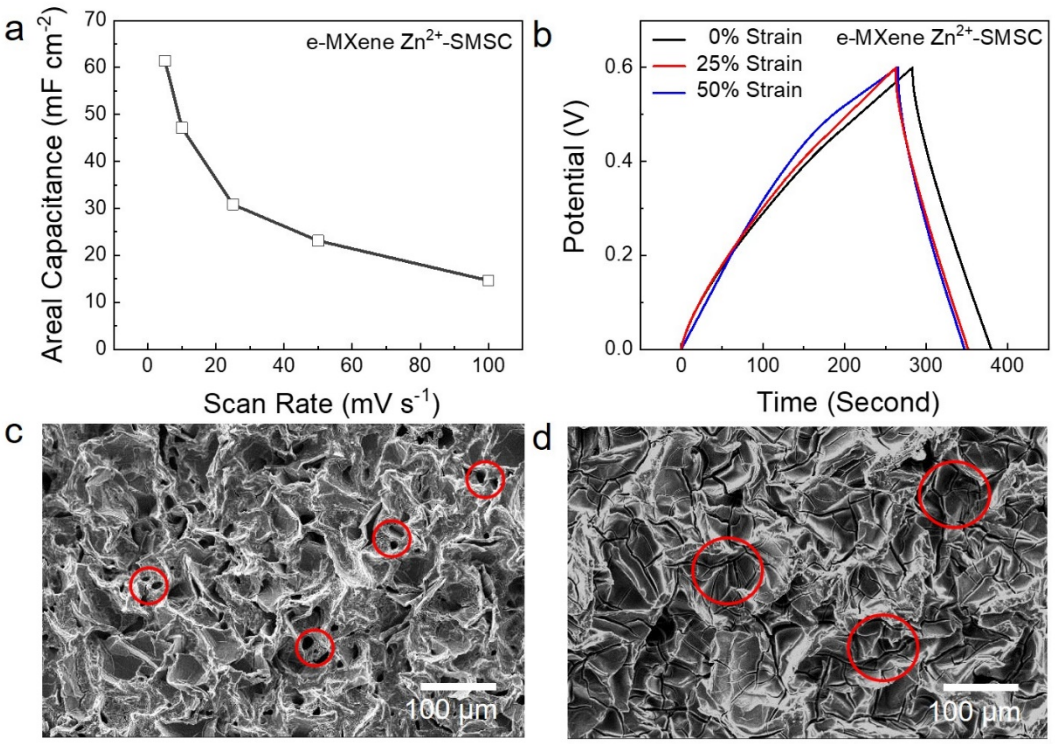

Fig S7. (a) C_A of an e-MXene Zn^{2+}-SMSC from 5 to 100 mV s^{-1}. (b) GCD profiles of an e-MXene Zn^{2+}-SMSC under different uniaxial strains (at 0.1 mA cm^{-2}). SEM images of the e-MXene electrodes of (c) Zn^{2+}-SMSC and (d) H^+-SMSC after 1,000 charge-discharge cycles. Several pinholes were observed on the e-MXene electrodes of Zn^{2+}-SMSC, and some cracks were noticed on the e-MXene electrodes of H^+-SMSC.

Table S1. Comparison of e-MXene H^+-SMSC and e-MXene Zn^{2+}-SMSC in this work with other MXene-based MSCs reported in the literature.

Devices or Electrodes (–)	Configuration of MSC (Working Window)	Stretchability/Flexible (Maximal Strain)	Electrolyte (Neutral, Acid, Base)	Current Collector	C_A (mF cm^{-2})	Ref.
e-MXene Zn^{2+}-SMSC	Symmetric (0.6 V)	Stretchable (50%)	Gelatin/1 M $ZnSO_4$ (Neutral)	No	61.4 @ 5 mV s^{-1}	This Work
e-MXene H^+-SMSC	Symmetric (0.6 V)	Stretchable (50%)	PVA/3 M H_2SO_4 (Acid)	No	127.9 @ 10 mV s^{-1}	This Work
N-Doped $Ti_3C_2T_x$ MXene	Symmetric (0.6 V)	Flexible (–)	PVA/3 M H_2SO_4 (Acid)	No	70.1 @ 10 mV s^{-1}	4
$Ti_3C_2T_x$ MXene	Symmetric (0.6 V)	Flexible (–)	PVA/1 M H_2SO_4 (Acid)	No	27.3 @ 20 mV s^{-1}	5
Printed $Ti_3C_2T_x$ MXene	Symmetric (0.6 V)	Flexible (–)	PVA/3 M H_2SO_4 (Acid)	No	43 @ 5 μA cm^{-2}	6
$Ti_3C_2T_x$-Bacterial Cellulose	Symmetric (0.6 V)	Stretchable (100%)	PVA/1 M H_2SO_4 (Acid)	Au Films	115.1 @ 2 mA cm^{-2}	7
Stamped I-$Ti_3C_2T_x$ MXene	Symmetric (0.6 V)	Flexible (–)	PVA/3 M H_2SO_4 (Acid)	No	61 @ 25 μA cm^{-2}	2
Stamped Y-$Ti_3C_2T_x$ MXene	Symmetric (0.6V)	Flexible (–)	PVA/3 M H_2SO_4 (Acid)	No	34 @ 25 μA cm^{-2}	2
rGO-MXene	Asymmetric (1.0 V)	Flexible (–)	PVA/1 M H_2SO_4 (Acid)	No	2.4 @ 2 mV s^{-1}	8
$Ti_3C_2T_x$ MXene	Symmetric (0.6 V)	Rigid (–)	PVA/1 M H_2SO_4 (Acid)	Au Films	27.29 @ 0.25 mA cm^{-2}	9
Laser-Cutting $Ti_3C_2T_x$ MXene	Symmetric (0.6 V)	Rigid (–)	PVA/1 M H_2SO_4 (Acid)	Au Films	71.16 @ 0.25 mA cm^{-2}	10
PEDOT-$Ti_3C_2T_x$ MXene	Symmetric (0.6 V)	Flexible (–)	PVA/1 M H_2SO_4 (Acid)	No	2.4 @ 10 mV s^{-1}	11
RuO_2-$Ti_3C_2T_x$ MXene	Asymmetric (1.5 V)	Rigid (–)	PVA/1 M H_2SO_4 (Acid)	Carbon Fabrics	60 @ 5 mV s^{-1}	12
SWCNT-MXene	Symmetric (0.6 V)	Flexible (–)	PVA/1M H_2SO_4 (Acid)	No	0.86 @ 2 μA cm^{-2}	13
$Ti_3C_2T_x$ MXene-CNF	Symmetric (0.6 V)	Flexible (–)	PVA/1 M H_2SO_4 (Acid)	No	25.3 @ 2 mV s^{-1}	14
MXene-Graphene Aerogel	Symmetric (0.6 V)	Flexible (–)	PVA/1 M H_2SO_4 (Acid)	No	34.6 @ 1 mV s^{-1}	15
PEDOT-$Ti_3C_2T_x$ MXene	Symmetric (0.6 V)	Flexible (–)	Graphene Oxide /PVA/H_2SO_4 (Acid)	No	40.8 @ 0.16 mA cm^{-2}	16

Freeze Thawed MXene	Symmetric (0.6 V)	Rigid (–)	PVA/1 M H_2SO_4 (Acid)	No	23.6 @ 20 mV s^{-1}	17
Ionic Liquid Intercalated $Ti_3C_2T_x$ MXene	Symmetric (3.0 V)	Flexible (–)	$EMIMBF_4$/PVDF-HFP	No	44 @ 0.1 mA cm^{-2}	18
Laser-Etched MXene	Symmetric (0.6 V)	Flexible (–)	PVA /1 M H_2SO_4 (Acid)	No	3.75 @ 0.1 mA cm^{-2}	19
Laser Writing MXene	Symmetric (0.6 V)	Rigid (–)	PVA/3 M H_2SO_4 (Acid)	No	11.8 @ 10 mV s^{-1}	20
Mn^{2+} Intercalated MXene	Symmetric (0.6 V)	Flexible (–)	PVA/1M H_3PO_4 (Acid)	No	87 @ 2 mV s^{-1}	21

Note: rGO – reduced graphene oxide; PEDOT – poly(3,4-ethylenedioxythiophene); RuO2 – ruthenium oxide; SWCNT – single wall carbon nanotube; CNF – cellulose nanofibrils; PVA – poly(vinyl alcohol); $EMIMBF_4$ – 1-butyl-3-methylimidazolium tetrafluoroborate; PVDF-HFP –poly(vinylidenefluoride-hexafluoropropylene).

Table S2. Comparison of e-MXene H^+-SMSC and e-MXene Zn^{2+}-SMSC in this work with other SMSCs reported in the literature.

Devices or Electrodes (–)	Configuration of SMSC (Working Window)	Electrolyte of MSCs (Neutral, Acid, Base)	Current Collectors	C_A (mF cm^{-2})	Stretchability	Ref.
e-MXene Zn^{2+}-SMSC	Symmetric (0.6 V)	Gelatin/1 M $ZnSO_4$ (Neutral)	No	61.6 @ 5 mV s^{-1}	50% Uniaxial	This Work
e-MXene H^+-SMSC	Symmetric (0.6 V)	PVA/3 M H_2SO_4 (Acid)	No	108.8 @10 mV s^{-1}	50% Uniaxial	This Work
MnO_2/CNT	Symmetric (0.8 V)	[BMIM][TFSI]/PMMA (Organic)	No	12.6 @ 5 mA cm^{-2}	30% Biaxial	22
(PEDOT:PSS)/ Graphene	Symmetric (0.8 V)	PVA/1 M H_2SO_4 (Acid)	No	19.3 @ 20 μA cm^{-2}	50% Uniaxial	23
N-doped graphene/ (PEDOT: PSS)	Symmetric (0.8 V)	PAAK/1 M KOH (Base)	No	0.79 @ 50 μA cm^{-2}	100% Uniaxial	24
rGO	Symmetric (0.8V)	PVA/2 M LiCl (Neutral)	Ni-Coated Fabrics	50.6 @ 10 mV s^{-1}	100% Uniaxial	25
rGO-MXene	Symmetric (1.0 V)	PVA/1 M H_2SO_4 (Acid)	No	18.6 @ 0.1 A g^{-1}	300% Uniaxial	26
MWCNT/Mn Mo Oxide	Symmetric (2.0 V)	ADN/SN/LiTFSI/PMMA (Organic)	Cr/Au	7.5 @ 0.3 mA cm^{-2}	50% Biaxial	27
Vertical AuNWs/PANI	Symmetric (0.8)	PVA/1 M H_3PO_4 (Acid)	No	5.03 @ 20 mV s^{-1}	100% Uniaxial	28
$Ti_3C_2T_x$/Bacterial Cellulose Kirigami	Symmetric (0.6 V)	PVA/1 M H_2SO_4 (Acid)	Au	111.5 @ 0.5 mA cm^{-2}	100% Uniaxial	7

Note: [BMIM][TFSI] – 1-butyl-3-methylimidazolium bis(trifluoromethylsulfonyl)imide; PMMA – poly(methyl methacrylate); PEDOT:PSS – poly(3,4-ethylenedioxythiophene):poly(4-styrenesulfonate); PAAK – potassium polyacrylate; ADN – adiponitrile; SN – succinonitrile; LiTFSI – lithiumbis(trifluoromethanesulfonyl)imide; AuNWs – gold nanowires; PANI – polyaniline.

Supplementary References

1. M. Ghidiu, M. R. Lukatskaya, M. Q. Zhao, Y. Gogotsi and M. W. Barsoum, *Nature*, 2014, **516**, 78-81.
2 C. J. Zhang, M. P. Kremer, A. Seral-Ascaso, S.-H. Park, N. McEvoy, B. Anasori, Y. Gogotsi and V. Nicolosi, *Adv. Funct. Mater.*, 2018, **28,**1705506.
3. Q. Yang, Z. Huang, X. Li, Z. Liu, H. Li, G. Liang, D. Wang, Q. Huang, S. Zhang, S. Chen and C. Zhi, *ACS Nano*, 2019, **13**, 8275-8283.
4. L. Yu, Z. Fan, Y. Shao, Z. Tian, J. Sun and Z. Liu, *Adv. Energy Mater.*, 2019, **9**, 1901839.
5. Y.-Y. Peng, B. Akuzum, N. Kurra, M.-Q. Zhao, M. Alhabeb, B. Anasori, E. C. Kumbur, H. N. Alshareef, M.-D. Ger and Y. Gogotsi, *Energy Environ. Sci.*, 2016, **9**, 2847-2854.
6. C. J. Zhang, L. McKeon, M. P. Kremer, S. H. Park, O. Ronan, A. Seral-Ascaso, S. Barwich, C. O. Coileain, N. McEvoy, H. C. Nerl, B. Anasori, J. N. Coleman, Y. Gogotsi and V. Nicolosi, *Nat. Commun.*, 2019, **10**, 1795.
7. S. Jiao, A. Zhou, M. Wu and H. Hu, *Adv. Sci.*, 2019, **6**, 1900529.
8. C. Couly, M. Alhabeb, K. L. Van Aken, N. Kurra, L. Gomes, A. M. Navarro-Suárez, B. Anasori, H. N. Alshareef and Y. Gogotsi, *Adv. Electron. Mater.*, 2018, **4**, 1900537.
9. H. Hu and T. Hua, *J. Mater. Chem. A*, 2017, **5**, 19639-19648.
10. H. Hu, Z. Bai, B. Niu, M. Wu and T. Hua, *J. Mater. Chem. A*, 2018, **6**, 14876-14884.
11. T. Cheng, Y. W. Wu, Y. L. Chen, Y. Z. Zhang, W. Y. Lai and W. Huang, *Small*, 2019, **15**, 1901830.
12. Q. Jiang, N. Kurra, M. Alhabeb, Y. Gogotsi and H. N. Alshareef, *Adv. Energy Mater.*, 2018, **8**, 1703043.
13. C. J. Zhang, B. Anasori, A. Seral-Ascaso, S. H. Park, N. McEvoy, A. Shmeliov, G. S. Duesberg, J. N. Coleman, Y. Gogotsi and V. Nicolosi, *Adv. Mater.*, 2017, **29**, 1702678.
14. W. Tian, A. VahidMohammadi, M. S. Reid, Z. Wang, L. Ouyang, J. Erlandsson, T. Pettersson, L. Wagberg, M. Beidaghi and M. M. Hamedi, *Adv. Mater.*, 2019, **31**, 1902977.
15. Y. Yue, N. Liu, Y. Ma, S. Wang, W. Liu, C. Luo, H. Zhang, F. Cheng, J. Rao, X. Hu, J. Su and Y. Gao, *ACS Nano*, 2018, **12**, 4224-4232.
16. P. Das, X. Shi, Q. Fu and Z. S. Wu, *Adv. Funct. Mater.*, 2019, **30**, 1908758.
17. X. Huang and P. Wu, *Adv. Funct. Mater.*, 2020, **30**, 1910048.
18. S. Zheng, C. Zhang, F. Zhou, Y. Dong, X. Shi, V. Nicolosi, Z.-S. Wu and X. Bao, *J. Mater. Chem. A*, 2019, **7**, 9478-9485.
19. Q. Li, Q. Wang, L. Li, L. Yang, Y. Wang, X. Wang and H. T. Fang, *Adv. Energy Mater.*, 2020, **10**, 2070104.
20. J. Tang, W. Yi, X. Zhong, C. J. Zhang, X. Xiao, F. Pan and B. Xu, *Energy Storage Mater.*, 2020, **32**, 418-424.
21. X. Feng, J. Ning, B. Wang, H. Guo, M. Xia, D. Wang, J. Zhang, Z.-S. Wu and Y. Hao, *Nano Energy*, 2020, 104741.
22. J. Yun, H. Lee, C. Song, Y. R. Jeong, J. W. Park, J. H. Lee, D. S. Kim, K. Keum, M. S. Kim, S. W. Jin, Y. H. Lee, J. W. Kim, G. Zi and J. S. Ha, *Chem. Eng. J.*, 2020, **387**, 124076.
23. W. Yan, J. Li, G. Zhang, L. Wang and D. Ho, *J. Mater. Chem. A*, 2020, **8**, 554-564.

24. W. Song, J. Zhu, B. Gan, S. Zhao, H. Wang, C. Li and J. Wang, *Small*, 2018, **14**, 1702249.
25. Z. Cong, W. Guo, Z. Guo, Y. Chen, M. Liu, T. Hou, X. Pu, W. Hu and Z. L. Wang, *ACS Nano*, 2020, **14**, 5590-5599.
26. Y. Zhou, K. Maleski, B. Anasori, J. O. Thostenson, Y. Pang, Y. Feng, K. Zeng, C. B. Parker, S. Zauscher, Y. Gogotsi, J. T. Glass and C. Cao, *ACS Nano*, 2020, **14**, 3576-3586.
27. G. Lee, J. W. Kim, H. Park, J. Y. Lee, H. Lee, C. Song, S. W. Jin, K. Keum, C. H. Lee and J. S. Ha, *ACS Nano*, 2019, **13**, 855-866.
28. T. An, B. Zhu, Y. Ling, S. Gong and W. Cheng, *J. Mater. Chem. A*, 2019, **7**, 14233-14238.